






Three-dimensional reconstructions of haustoria in two parasitic plant species in the Orobanchaceae

Natsumi Masumoto,¹ Yuki Suzuki ,^{2,3,†} Songkui Cui,^{4,*†} Mayumi Wakazaki,⁵ Mayuko Sato ,⁵ Kie Kumaishi,⁶ Arisa Shibata,⁵ Kaori M. Furuta,⁴ Yasunori Ichihashi,⁶ Ken Shirasu ,^{5,7} Kiminori Toyooka ,⁵ Yoshinobu Sato² and Satoko Yoshida ,^{1,4,*†}

- 1 Division of Biological Science, Graduate School of Science and Technology, Nara Institute of Science and Technology, Nara, 630-0192, Japan
- 2 Division of Information Science, Graduate School of Science and Technology, Nara Institute of Science and Technology, Nara, 630-0192, Japan
- 3 Graduate School of Information Science and Technology, Osaka University, Osaka, 565-0871, Japan
- 4 Division for Research Strategy, Institute for Research Initiatives, Nara Institute of Science and Technology, Nara, 630-0192, Japan
- 5 RIKEN Center for Sustainable Resource Science, Yokohama, 230-0045, Japan
- 6 RIKEN BioResource Research Center, Ibaraki, 305-0074, Japan
- 7 Graduate School of Science, The University of Tokyo, Tokyo, 113-0033, Japan

*Author for communication: satokoy@bs.naist.jp

†Senior authors.

‡Present address: Graduate School of Medicine, Osaka University, Osaka, Japan.

S.C. and S.Y. conceived the idea of this study, designed the experiment, analyzed the data, and wrote the manuscript. N.M. was responsible for color coding, FE-SEM, and 3-D reconstruction. Y.Su. and Y.Sa. developed methods to align section images, automated the color coding process, and provided crucial technical assistance for 3-D reconstruction. Y.I., A.S., and K.K. assisted with image handling. K.T., M.W., and M.S. prepared serial thin sections and performed FE-SEM. K.M.F. analyzed the *AtPEAR* promoter. K.S. provided critical comments on the manuscript.

The author responsible for distribution of materials integral to the findings presented in this article in accordance with the policy described in the Instructions for Authors (<https://academic.oup.com/plphys/pages/general-instructions>) is: Satoko Yoshida (satokoy@bs.naist.jp).

Abstract

Parasitic plants infect other plants by forming haustoria, specialized multicellular organs consisting of several cell types, each of which has unique morphological features and physiological roles associated with parasitism. Understanding the spatial organization of cell types is, therefore, of great importance in elucidating the functions of haustoria. Here, we report a three-dimensional (3-D) reconstruction of haustoria from two Orobanchaceae species, the obligate parasite *Striga hermonthica* infecting rice (*Oryza sativa*) and the facultative parasite *Phtheirospermum japonicum* infecting *Arabidopsis* (*Arabidopsis thaliana*). In addition, field-emission scanning electron microscopy observation revealed the presence of various cell types in haustoria. Our images reveal the spatial arrangements of multiple cell types inside haustoria and their interaction with host roots. The 3-D internal structures of haustoria highlight differences between the two parasites, particularly at the xylem connection site with the host. Our study provides cellular and structural insights into haustoria of *S. hermonthica* and *P. japonicum* and lays the foundation for understanding haustorium function.

Introduction

Parasitic plants are vascular plants that invade host plant tissues to acquire water and nutrients from their hosts. Plant

parasitism independently evolved at least 12 times (Bennett and Mathews, 2006). Approximately 4,500 species in 28 families, representing 1% of all angiosperm species, are proposed

to be parasitic plants (Westwood et al., 2010; Heide-Jørgensen, 2013). The common feature of parasitic plants is the ability to form a specialized invasive organ called a haustorium. Unlike the unicellular haustoria found in plant-infecting pathogenic fungi, haustoria in parasitic plants are multicellular organs that function in host attachment, host tissue invasion, and establishing a vascular connection between the parasite and host for material transfer (Yoshida et al., 2016). Haustoria facilitate water and nutrient acquisition as well as translocation of RNA molecules, peptides, and plant hormones between the host and parasite (Kim et al., 2014; Spallek et al., 2017; Shahid et al., 2018; Liu et al., 2019; Yoshida et al., 2019). Thus, haustoria act as efficient biological channels for interspecies material transfer, but the internal structures and physiological functions of haustoria are largely unexplored.

The Orobanchaceae family contains the largest number of root parasitic species and presents various degrees of host dependency. An exception among Orobanchaceae family members is in the genus *Lindenbergia*, of which all species are non-parasitic plants (Hjertson, 1995). Facultative parasites, including those in the genera *Triphysaria*, *Phtheirospermum*, and *Rhinanthus*, are able to live as autotrophs and reproduce seeds without a host but will parasitize hosts when available. Obligate parasitic plants, including those in the genera *Striga*, *Orobanche*, and *Phelipanche*, cannot complete their life cycles in nature without a host. Some of the obligate parasites in the Orobanchaceae represent major agricultural threats because they parasitize important staple crops. For example, *Striga hermonthica*, commonly known as witchweed, infests rice, maize (*Zea mays*), sorghum (*Sorghum bicolor*), sugarcane (*Saccharum officinarum*), and pearl millet (*Cenchrus americanus*), affects millions of smallholder farmers in sub-Saharan Africa, and, thus, has a large impact on global food security (Spallek et al., 2013; Runo and Kuria, 2018; Mutuku and Shirasu, 2019).

Haustorial morphology varies depending on the species. Facultative parasitic plants form lateral haustoria that develop on the sides of roots without permanently stopping meristematic activity of the roots. In contrast, obligate parasitic plants form terminal haustoria at the radicle tips by deforming the root apical meristem (Westwood et al., 2010; Yoshida and Shirasu, 2009). These obligate parasites have small seeds with limited nutrient reserves (Joel et al., 2012); thus, nutrient acquisition through terminal haustoria is crucial for the survival of obligate parasites. Some obligate parasites, such as *Striga*, are also able to form lateral haustoria on their secondarily emerged adventitious roots after successful establishment of a host connection via a terminal haustorium.

Despite the evidence for distinct haustorium types, the developmental processes and major internal cell structures are similar between lateral and terminal haustoria in the Orobanchaceae. The initial formation of a haustorium is provoked by host-derived small compounds, collectively

called haustorium-inducing factors (HIFs; Goyet et al., 2019). The HIF signals induce cell division and cell deformation as well as the extension of epidermal cells on the haustorium-forming site, called haustorial hairs (or papillae), that function in host attachment (Cui et al., 2016). Upon host contact, haustoria develop intrusive cells at their apex, acting at the front line of host penetration. *Phtheirospermum japonicum* ethylene signaling mutants exhibit strong defects in intrusive cell formation as well as host penetration, indicating the importance of the intrusive cell formation in host penetration (Cui et al., 2020). The intrusive cells penetrate host tissues toward the host's stele and show palisade alignment against host xylem strands. Therefore, these cells are sometimes referred as palisade cells or endophyte (Musselman and Dickison, 1975). After successful entry into the host's vascular system, parts of the intrusive cells differentiate into tracheary elements (TEs). In parallel, a mass of TE, called plate xylem or vascular core, develop in the basal region of the haustorium (Musselman and Dickison, 1975; Heide-Jørgensen and Kuijt, 1995). These two types of xylem tissues are eventually connected in the middle of the haustorium to form a xylem bridge that facilitates molecular flow between the parasite and its host (Ishida et al., 2016; Wakatake et al., 2018).

During the haustorium development processes, each root cell layer starts cell division to contribute to haustorium expansion, and the original root cell identities, such as endodermis and epidermis, are lost. This is supported by diminishment of endodermis and epidermis marker gene expression in haustorial cells in the facultative parasite *P. japonicum* (Cui et al., 2016; Wakatake et al., 2018). Instead, haustorial cells acquire new cellular identity; the epidermis-originated intrusive cells express intrusive-cell specific genes including *INTRUSIVE CELL-SPECIFIC LEUCINE-RICH REPEAT RECEPTOR-LIKE KINASE 1* (*ICSL1*), *GERMIN-LIKE PROTEIN 1* (*GLP1*), and several Group1 subtilase-encoding genes (*SBTs*; Ogawa et al., 2021). In the central part of a haustorium of *P. japonicum*, small cells surrounding the xylem bridge express procambium marker genes, such as homologs of *Arabidopsis* (*Arabidopsis thaliana*) *HOMEBOX PROTEIN 15* (*HB15a*), *HB18*, and *WUSCHEL-RELATED HOMEBOX 4* (*WOX4*). Thus, these cells are called procambium-like cells (Wakatake et al., 2018). After a host–parasite vascular connection is established, a cluster of parenchyma cells, called the hyaline body and also referred to as parenchyma core or central core, are observed in many species, including the obligate parasites *Striga* and *Alectra*, as well as the facultative parasite *Rhinanthus* (Kuijt, 1977; Visser et al., 1984; Pielach et al., 2014). Hyaline cells forming the hyaline body have a dense cytoplasm enriched with organelles and have extracellular depositions (Visser et al., 1984; Pielach et al., 2014). Because hyaline bodies appear only in compatible host–parasite interactions, their roles have been postulated as being important for later stages of parasitic plant growth (Gurney et al., 2006; Pielach et al., 2014).

The structure of the vascular connection between hosts and parasites varies depending on the species (Smith et al., 2013). An obligate parasite *S. hermonthica* and a facultative parasite *Rhinanthus minor* were reported to form oscula, tubular structures that directly penetrate host xylem vessels to form a conduit connection between the host and parasite (Dörr, 1997; Cameron et al., 2006); whereas *Orobancha crenata* connects to host xylems by open pits (Dörr and Kollmann, 1976). A phloem connection has been reported in the holo (non-photosynthetic) parasitic species *O. crenata* and *Orobancha cumana* (Dörr and Kollmann, 1995; Krupp et al., 2019). In contrast, no phloem cells were detected in the host contact sites of haustoria in hemi (photosynthetic) parasites, including the obligate *Striga* and *Alectra* spp., as well as the facultative *Triphysaria* (Dörr et al., 1979; Ba, 1988; Heide-Jørgensen and Kuijt, 1993; Dörr, 1997; Kokla and Melnyk, 2018).

Although many histological studies and electron micrographs are available documenting host and parasitic plant interaction, the spatial relationship between host and parasite cells is not well understood. To overcome this issue, we have developed complete three-dimensional (3-D) images of haustoria. Although fluorescence images taken by confocal microscopy are widely used for reconstructing 3-D images, this approach is challenging to use for haustoria due to their thick tissues. In addition, haustorial cell type-specific gene markers have not yet been fully identified in parasitic plants. Thus, we constructed 3-D images of haustoria from serial thin sections of *S. hermonthica* and *P. japonicum* and visualized individual cell types inside haustoria interacting with their hosts.

Results

3-D reconstruction approach

To reconstruct 3-D images of haustoria, we collected haustoria of the obligate parasite *S. hermonthica* infecting rice for 14 d and the facultative parasite *P. japonicum* infecting *Arabidopsis* for 9 d (Figure 1, A and B). These haustoria, respectively, represent fully matured terminal and lateral haustoria, as previous studies showed that *S. hermonthica* and rice establish their vascular connection within 7 d (Yoshida et al., 2019) and *P. japonicum* and *Arabidopsis* do so within 3 d of interaction (Wakatake et al., 2018). Because each haustorium was approximately 400 μm in size, which is beyond the depth of focus in an ordinary fluorescence laser scanning confocal microscopy, we decided to approach reconstruction using physical serial thin sections.

The workflow for 3-D reconstruction is shown in Figure 1, C. Preparation of serial thin sections with 1- μm thickness resulted in 526 and 378 sections from haustoria of *S. hermonthica* and *P. japonicum*, respectively. Among them, 374 consecutive sections of *S. hermonthica* and all sections of *P. japonicum* were used for further analysis. Because each section was manually placed on a glass slide, the positions and angles of each image varied among the

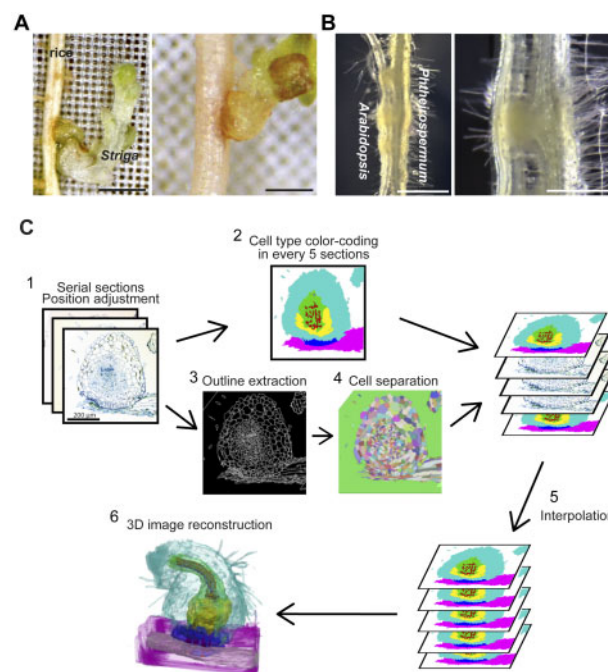


Figure 1 3-D reconstructions of *S. hermonthica* and *P. japonicum* haustoria. A, Representative image of *S. hermonthica* 2 weeks after infection of a rice root. A magnified image of a terminal haustorium is shown in the right panel. B, Representative image of a *P. japonicum* root 9 d after infection of an *Arabidopsis* root. Right panel shows the magnified image of a lateral haustorium. Scale bars: left panels in A and B = 1 mm; right panels in A and B = 500 μm . C, Workflow of 3-D reconstruction. 1. Tissue preparation, sectioning, staining, photographing, and aligning image position. 2. Manual painting of each cell type in every fifth image. 3. Extraction of cell outline in all sections. 4. Segmentation of each cell in all sections. 5. Automated color coding of the unpainted images, based on manually painted images using automated interpolation. 6. Reconstruction of 3-D haustorial structure.

sections. In addition, some sections had wrinkles and unequal staining that caused non-rigid deformation. To obtain aligned and continuous tissue images, we applied intensity-based rigid image registration using an image registration library (Marstal et al., 2016) and intensity-based non-rigid image registration to the images having wrinkled sections. The cells in the aligned images were labeled with different color codes according to cell types defined in the following sections. Since manually labeling cells in every section image is time consuming, we developed a semi-automated labeling method. In brief, color codes were manually painted on every fifth image and the rest of the images was labeled by an automated interpolation algorithm (Figure 1, C and Supplemental Figure S1). The resulting color images were manually checked and painting mistakes were corrected. Finally, all painted images were stacked to form a 3-D image and converted into polygon meshes that represent the surface structures of cell types (for details, see the “Materials and methods” section).

Defining cell types in a *S. hermonthica* haustorium infecting a rice root

For color-coding of cell types, we categorized the *S. hermonthica* haustorial cells into six cell types: peripheral cells, hyaline cells, procambium-like cells, intrusive cells, TEs, and sieve elements (SEs; Figure 2, A). Host rice cells were categorized into two groups: vascular cells that include xylem, phloem, and procambium, and outer cells that include endodermal, cortical, and epidermal cells (Figure 2, A). In section images, larger cells in the periphery of the haustorium and smaller cells in the center of the haustorium were observed. Larger cells at the haustorium's periphery consist of epidermis and cortical (or peripheral parenchyma) cells that have vacuolated intracellular structures (Figure 2, A, B, H, and K; Heide-Jørgensen and Kuijt, 1995). We labeled these cells as peripheral cells. Smaller cells at the center of the haustorium contained five cell types, including hyaline body, procambium-like cells, intrusive cells, TE, and SE (Figure 2, A). The following morphological characteristics were used as criteria for defining different cell types of these smaller cells, and each cell type was observed using field-emission scanning electron microscopy (FE-SEM) to confirm intracellular structures (Figure 2).

Hyaline cells, constituting the hyaline body, were stained light blue by toluidine blue. The extracellular spaces of hyaline cells were stained dark blue by toluidine blue and contained highly electron dense material as observed by FE-SEM, indicating extracellular deposits, a typical feature of hyaline bodies (Figure 2, B–D). FE-SEM analysis revealed that the cytosol of hyaline cells was densely occupied by irregular membrane structures, likely thickened smooth endoplasmic reticulum (ER; Figure 2, D and E).

Small and round cells at the center of the haustorium missing the feature of hyaline cells were defined as procambium-like cells, according to the positional and morphological similarities with *P. japonicum* procambium-like cells, in which a set of procambium marker genes are expressed (Wakatake et al., 2018). Compared with hyaline cells, procambium-like cells displayed a lighter cytosolic density, contained fewer ER structures, and had a tight membrane contact with each other (Figure 2, B, C, and F). In 2-week-old *S. hermonthica*, the tissue above the haustorium has undergone lateral expansion and become a shoot. Because procambium cells in the *Striga* shoot are also small and morphologically indistinguishable from haustorial procambium-like cells on section images, we applied the same color to both cell types. Intrusive cells were characterized by their slender cell shape and palisade-like alignment against host vasculatures (Figure 2, H–J).

TEs are dead cells with thick secondary cell walls, recognized by their empty lumen and pitted outline (Figure 2, F and I). Differentiating TE had only an empty lumen (DTE in Figure 2, I). Some TE directly penetrated host xylem vessels and formed structures previously described as oscula (Figure 2, H and L; Dörr, 1997). A specialized type of haustorial TE called phloeotracheids that contain many tiny granules was previously reported (Dobbins and Kuijt, 1973;

Fineran, 1974; Musselman and Dickison, 1975), but we could not detect any granules inside haustorial TE in this study. Cell wall continuity between haustorial TE and host vessels was frequently observed at the host–parasite interface (Figure 3, A). SE showed less condensed cytoplasm and thickened cell walls. FE-SEM analysis detected characteristic plastid structures (Figure 2, C and G), called sieve-element plastids in SE cells (Behnke, 1991). We observed SE cells near the procambium-like cells in the basal region of the haustorium, but not in the central part of the haustorium (Figure 2, A and C).

3-D visualization of the internal structure of a *S. hermonthica* haustorium

3-D images of haustorium were recovered from stacks of cell-type labeled images. Opaque 3-D images clearly showed haustorial hairs at the surface of the haustorium, indicating the successful alignment of the serial sections in our experimental system (Figure 4, A and Supplemental Movie S1). The semi-translucent 3-D image highlighted the internal structure of a haustorium (Figure 4, B and Supplemental Movie S2). Xylem strands were continuous from the xylem vessels of a *Striga* shoot to the plate xylem and the xylem bridge in the haustorium (Figure 4, C–E and Supplemental Movie S3). Procambium-like cells and procambium cells surrounded the xylem strands (Figure 4, C and D and Supplemental Movie S3). Plate xylem formed a single aggregate at the base of the haustorium, and below that, 10 xylem bridges seamlessly connected to the host xylem cells (Figure 4, E). Interestingly, interface xylem cells appeared to bend their tips outward along the longitudinal axis of the host's vasculature (Figure 4, E). A hyaline body assumed a ring shape surrounding procambium-like cells (Figure 4, C, D, and F). Intrusive cells constituted the outermost layer of the haustorial apex region and covered most of interface area (Figure 4, B and D). Inside a *Striga* shoot, a few SE cell files extended in parallel with the shoot xylem. The tips of SE files were located above the xylem bridge in the vicinity of the plate xylem (Figure 4, C and D).

Defining cell types in a *P. japonicum* haustorium infecting *Arabidopsis* roots

For visualization of the internal structure of a haustorium of *P. japonicum* infecting *Arabidopsis*, we observed the cellular structure of the *P. japonicum* haustorium in serial sections by toluidine blue staining and by FE-SEM. We applied the same cell-type categories as *S. hermonthica* except hyaline cells, because hyaline cells were not apparent in the *P. japonicum* haustorium. Instead, cells with a dense cytosol, enriched organelles, and thickened primary cell walls were observed next to the xylem bridge (Figure 5, A–D). These cells have been also found in other facultative parasites, including *Triphysaria*, *Rhinanthus*, *Odontites*, and *Melampyrum*, and were previously described as paratracheal parenchyma (PP; Heide-Jørgensen and Kuijt, 1995; Pielach et al., 2014). Thus, we defined six cell types in the *P. japonicum* haustorium, i.e.

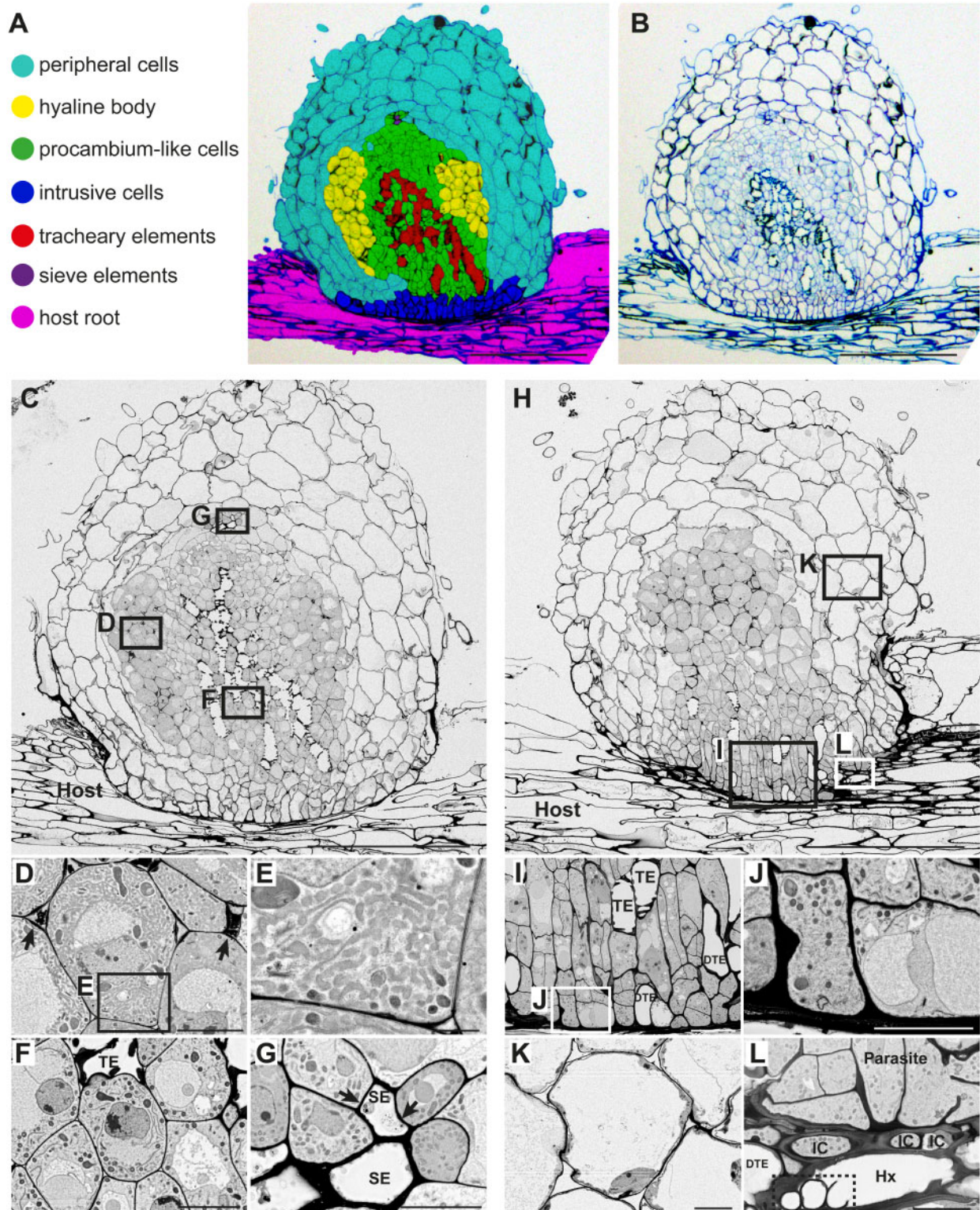


Figure 2 Tissue distribution and morphological characteristics of haustorial cells in *S. hermonthica*. A, Distribution of cell types in a *S. hermonthica* haustorium 2 weeks after infection of a rice root. B, Original toluidine blue-stained section used in A. C, A FE-SEM image in the center of a haustorium with a focus on the xylem bridge. D, A magnified image of hyaline cells from C, showing the accumulation of electron dense extracellular materials (arrows) between hyaline cells. E, Magnification of square box in D showing smooth-ER like structures in the cytosol of a hyaline cell. F, A magnified image from C showing procambium-like cells that surround a TE. G, A magnified image of SEs from C. Phloem plastids (arrows) were observed. H, A FE-SEM image of a haustorium section with a focus on intrusive cells. I, A magnified image of intrusive cells from H. DTE: differentiating TE. J, Magnification of square box in I showing cell wall thickening at the interface between parasite and host. K, A magnified image of haustorial cortical cells from H. L, A magnified image from H showing oscula structures (dashed box) inside a host vessel element (Hx), which is surrounded by three intrusive cells (ICs) and a DTE. Scale bars, A–C, H = 200 μ m; D, F, G, and J–L = 10 μ m; E = 2 μ m; and I = 20 μ m.

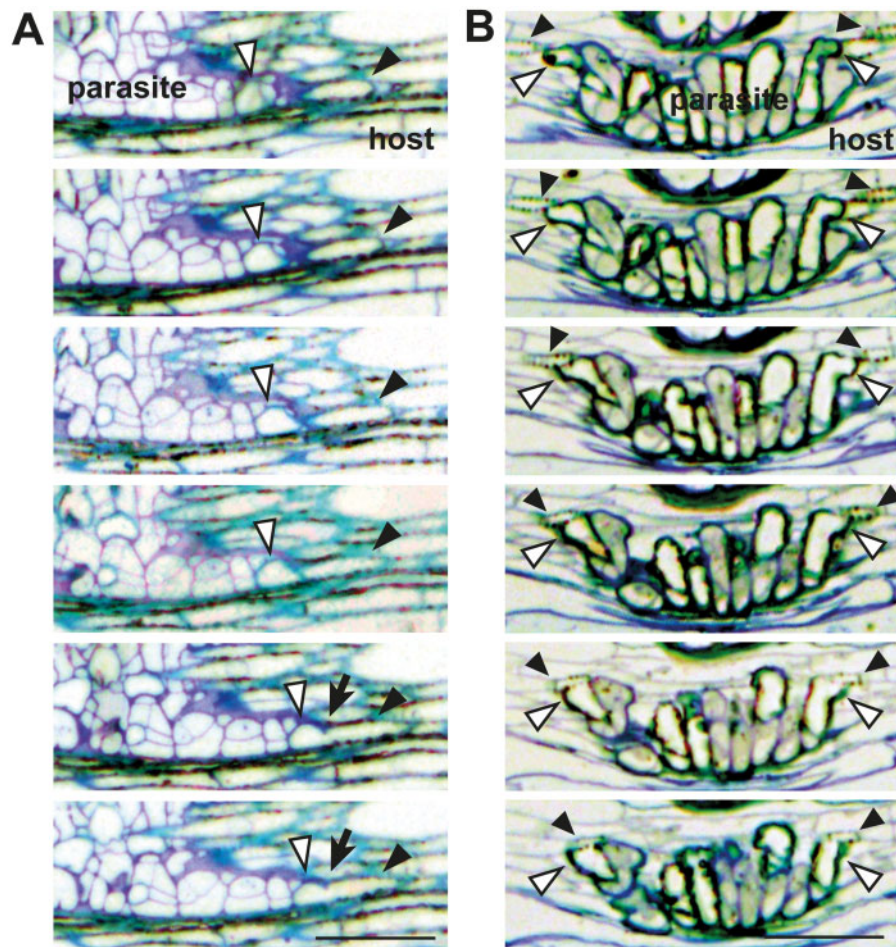


Figure 3 Interaction of parasite TEs with host xylem at the interface. A, Continuous section images of the *S. hermonthica*–rice interface showing cell wall continuity (arrows) between a TE of *S. hermonthica* haustorium and rice xylem. B, Continuous section images of the *P. japonicum*–*Arabidopsis* interface. Cell wall continuity was not observed at the attachment sites between the host xylem and parasite TE. White arrowheads: parasite TE. Black arrowheads: host xylem. Scale bars, 50 μ m.

peripheral cells (Figure 5, A), PP (Figure 5, D), procambium-like cells (Figure 5, F–H), intrusive cells (Figure 5, J and K), TE (Figure 5, D), and SE (Figure 5, L and M).

Procambium-like cells in *P. japonicum* were highly vacuolated and surrounded the PP and TE in the center (Figure 5, A–C). Detailed observations on the subcellular contents showed that these procambium-like cells can be divided into two groups (Figure 5, F). Those at the base and center of the haustorium (shown in red, Figure 5, F) were occupied by large vacuoles that contain many single- and multi-membrane small vesicles (Figure 5, G). Membrane invaginations were often observed adjacent to the vacuole membrane (arrowheads, Figure 5, G), indicating that the cytosolic matrix and organelles are actively degraded in these cells. In contrast, those located proximally to the host (blue color, Figure 5, F) had a relatively large cytosolic area that accumulated many atypical, unknown single-membrane structures (Figure 5, H). Higher magnification of intrusive cells at the host–parasite interface showed that, in some cases, each of these palisade-

like elongated cell structures contains several cells surrounded by thin cell walls (Figure 5, K).

Unlike *S. hermonthica*, oscula structures were not observed at the invasion site (Figure 3, B). Cell wall continuity between the interface xylem and host vessel elements was not found at the interface (Figure 3, B and Supplemental Figure S2), indicating that intrusive cells of *P. japonicum* do not penetrate *Arabidopsis* xylem. SEs were observed in the haustorium but only near the plate xylem (Figure 5, L and M). We could not determine whether these SE made continuity with root SE in the section images because of the difficulty in finding root SE in longitudinal sections.

3-D visualization of the internal structure of a *P. japonicum* haustorium

The 3-D model of a *P. japonicum* haustorium (Figure 6 and Supplemental Movies S4–S6) revealed that the haustorial surface is densely covered with haustorial hairs (Figure 6, A). Analysis of the surface structure highlighted the structural differences between haustorial hairs and root hairs. Root hairs facing toward the host roots (haustorial hairs) are

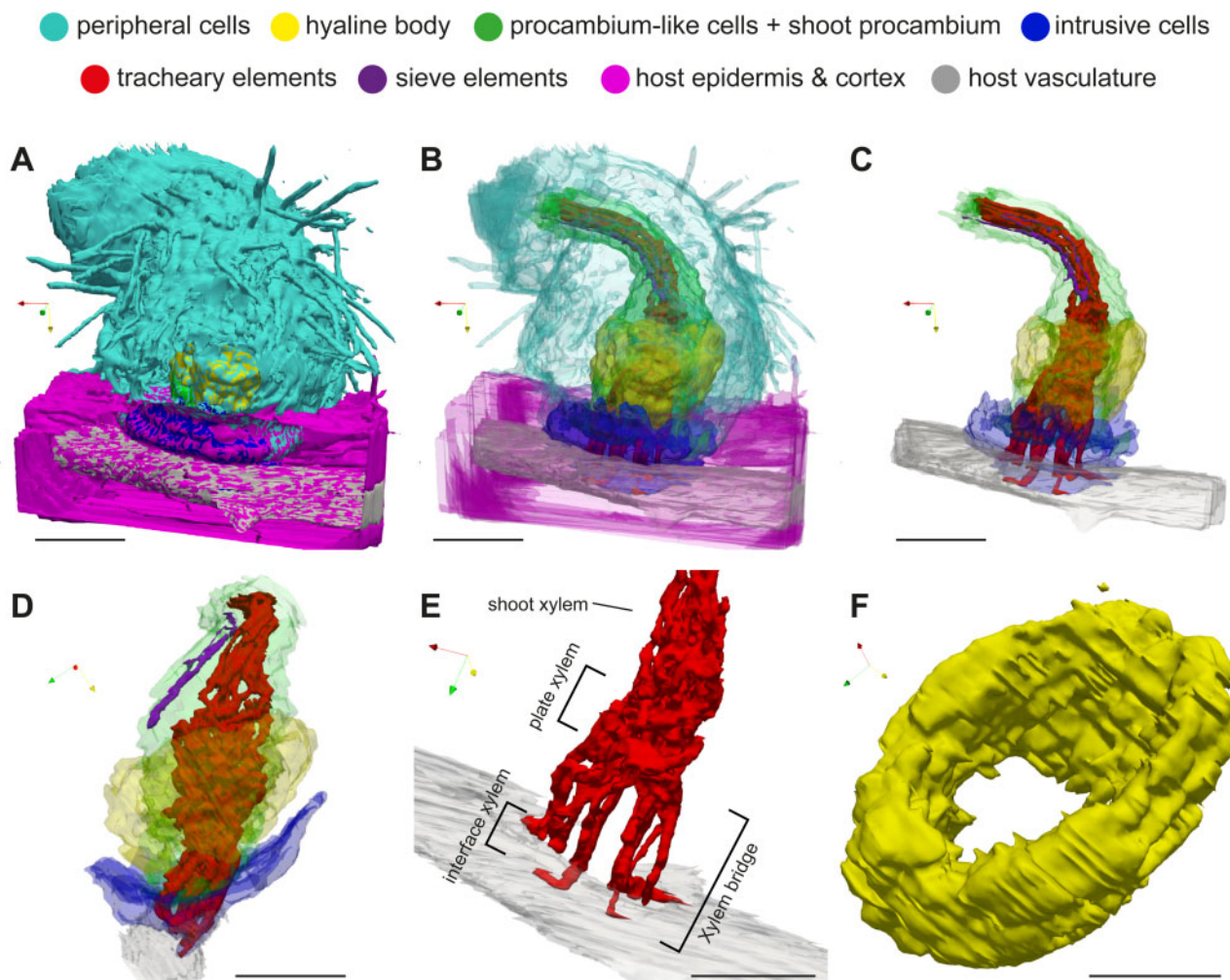


Figure 4 3-D images of a *S. hermonthica* haustorium. A, Surface structure. B, Semi-transparent view of the haustorium and host root. C and D, Internal haustorial cells and host root vasculature from the front (C) and side (D) views, respectively. E, A close-up view of the interface xylem, plate xylem, and shoot xylem of *Striga* with host vasculature. F, Close up view of a hyaline body forming a donut-shaped structure. X-, Y-, and Z-axes are indicated by red, yellow, and green arrows, respectively. Scale bars, A–E = 100 μ m; F = 50 μ m. Note that the scale bars in 3-D figures indicate the length on the horizontal XY plane.

wavy and thicker with a higher density compared with the hairs located opposite the host roots (root hairs), which are thinner and straight (Supplemental Movie S4). Some haustorial hairs appeared to stick to the host surface and be firmly attached to the host root, supporting the notion that haustorial hairs are recruited for host attachment (Cui et al., 2016). Plate xylem was observed at the base of the haustorium near the *P. japonicum* root xylem, and a single-stranded xylem bridge connected to four interface xylem strands that interacted with the host xylem (Figure 6, D and E). Interestingly interface xylem cells did not have straight contact with host xylem but assumed an arc shape to wrap around the host xylem (Figure 6, D and E). The middle of the xylem bridge was encircled by PP cells, whereas the rest of the xylem bridge and the plate xylem were surrounded by procambium-like cells (Figure 6, C). Similar to *S. hermonthica*, intrusive cells of *P. japonicum* covered the host's surface at the site where the haustorium first interacted with the host (Figure 6, F). SE with typical phloem plastids

were detected in the haustorium as two small clusters around the xylem plate at the outer boundary of procambium-like cells (Figure 6, G and H).

Since we were not able to identify *P. japonicum* root SE in our experimental system, the continuity of haustorial SE with root SE could not be resolved in 3-D. To answer this question, we expressed an SE marker construct, *pAtPEAR1::tdTomato-nls*, in which the Arabidopsis PHLOEM EARLY DOF 1 (*AtPEAR1*) promoter was fused with a *tdTomato* red fluorescent protein gene and a nuclear localization signal in *P. japonicum* hairy roots (Figure 6, I and J). In Arabidopsis, *PEAR1* is specifically expressed in protophloem SE (Miyashima et al., 2019). In *P. japonicum* hairy roots, the fluorescence signal was observed in the longitudinal cell files within the root vasculature (Figure 6, I), indicating that this construct can serve as a SE marker in *P. japonicum*. A number of haustorial cells next to the plate xylem also expressed the marker gene, giving rise to a similar SE distribution

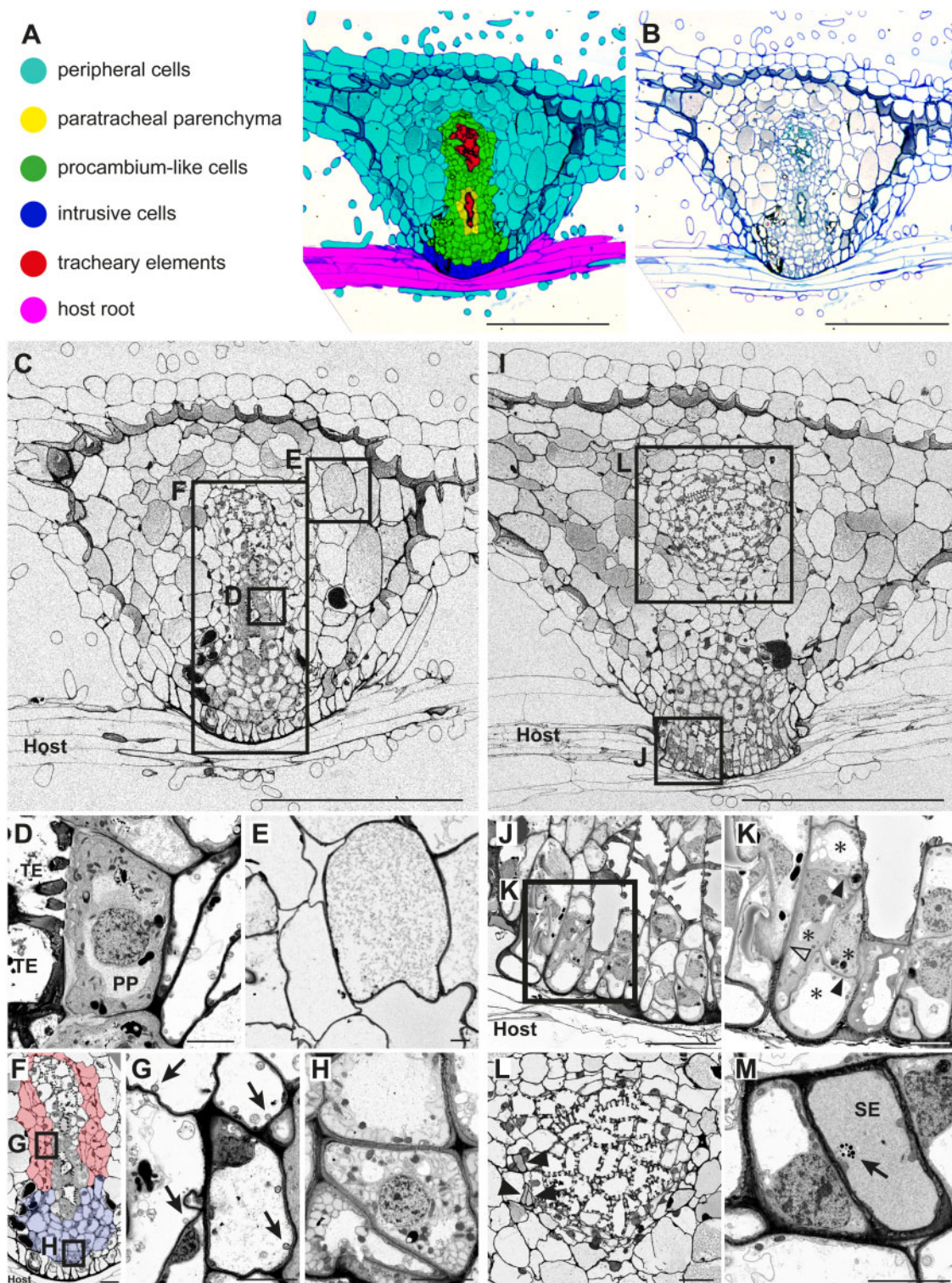


Figure 5 Tissue distribution and subcellular characteristics of cell types in a *P. japonicum* haustorium. A, Distribution of each cell type in a haustorium 9 d after infection of an *Arabidopsis* root. B, Original toluidine blue-stained section image used in A. C, A FE-SEM image at the center of the haustorium with the focus on the xylem bridge. D, A magnified image of PP and TEs from C. E, A magnified image of cortex cells from C. F, A magnified image of the haustorial center from C showing procambium-like cells (marked by blue and red color). Different colors denote different types of procambium-like cells. G, Magnification of the square box in F. Arrows indicate vacuolar membrane invaginations. H, Magnification of the square box in F showing atypical membrane structures in the cytosol of the procambium-like cells. I, A FE-SEM image of a haustorium section with the focus on intrusive cells. J, A magnified image of intrusive cells from I. K, Further magnification of intrusive cells from J. Note that four cells (asterisks) with thin cell wall (closed arrowheads) constitute an elongated cell shape that is enclosed by thicker cell wall (open arrowhead). L, A magnified image showing plate xylem and SEs (arrowheads). L is derived from an independent section, and its corresponding position in the haustorium is indicated in I. M, Magnification of the top most SE in L. A phloem plastid (arrow) was observed. Scale bars, A–C, and I = 200 μm ; F, J, and L = 20 μm ; D, E, G, H, K, and M = 5 μm .

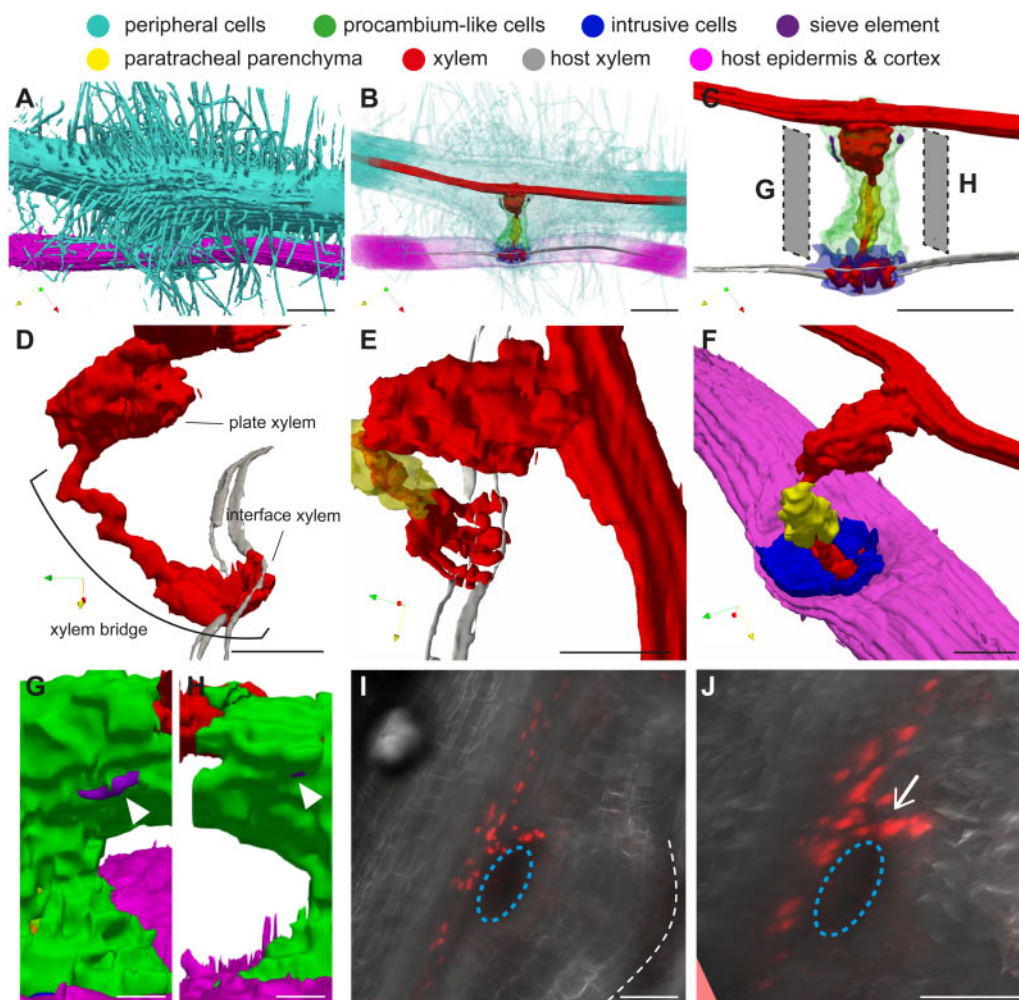


Figure 6 3-D images of a *P. japonicum* haustorium. A, Surface view showing attachment of many haustorial hairs on a host root. B, Semi-transparent view of a haustorium and the host root. C, Internal haustorial cells and host root vasculature. D and E, Close-up view of a xylem bridge interacting with the host's xylem visualized from side (D) and top (E). F, Close-up view showing that intrusive cells cover the entire interaction surface with the host. G and H, Localization of SEs (white arrowheads) in procambium-like cells. Visualization angles of G and H are indicated in C. I, Stacked confocal microscopy image for the expression of SE marker *pAtPEAR1::tdTomato-nls* (red signals) at 14 d after infection. White dashed line indicates the interface between haustorium and host. Blue dashed circles indicate the position of plate xylem. J, Visualization of I from a slightly different angle. Note that the nucleus-derived red signals form a continuous strand (white arrow) from those in the main vascular, indicating that haustorial SE is connected to root SE. X-, Y-, and Z-axes are indicated by red, yellow, and green arrows, respectively, in each 3-D image. Scale bars, A–C = 100 μm ; D–F, I, and J = 50 μm ; G and H = 20 μm . Note that the scale bars in 3-D figures indicate the length on the horizontal XY plane.

pattern to that observed in our 3-D image (Figure 6, C and I). This observation strongly supports the hypothesis that SEs are present in the haustorium in the vicinity of the plate xylem. Notably, the fluorescence signal appeared to be continuous at the junction between the parasite's root and the haustorium, indicating that haustorial SEs are connected to root SE.

Discussion

Following the first anatomical investigation of a parasitic plant haustorium by Bowman (1833), a considerable number of reports have shown the ultrastructure and histology of this evolutionarily interesting multicellular organ adapted for invasion of other plants (Fineran, 1974; Kuijt, 1977;

Heide-Jørgensen, 1991; Heide-Jørgensen and Kuijt, 1995; Dörr, 1997). Those studies provided valuable insights into cellular pattern and development of haustoria in a wide range of parasitic plant families. To extend our knowledge, we examined the spatial arrangement of cell types within the haustoria of two closely related Orobanchaceae species, *S. hermonthica* and *P. japonicum*. 3-D visualization of haustoria combined with detailed intra-cellular observations revealed the characteristics of each cell type.

Hyaline body and PP cells

The most prominent difference in the haustorial structure between the two species of parasitic plants was the presence or absence of a hyaline body. The hyaline body in

S. hermonthica infecting rice formed a ring-shaped thick layer surrounding the procambium-like cells and the xylem bridge. In contrast to *S. hermonthica*, we did not observe such a hyaline body in *P. japonicum*, in which there were no cells with large intercellular spaces accumulating extracellular deposits or with organelle-rich dense cytoplasm. Instead, we observed PP cells that were located along a xylem bridge and had dense cytoplasm and thick primary cell walls at the interface with xylem elements. Similar cells are present in other facultative parasites, including *R. minor*, *Odontites vernus*, *Melampyrum pratense* (Pielach et al., 2014), and *Triphysaria versicolor* (Heide-Jørgensen and Kuijt, 1995). Similar terms, such as plasma-rich parenchyma cells in the obligate parasite *O. crenata* (Dörr and Kollmann, 1976) and PP in *S. hermonthica*, have also been reported (Olivier et al., 1991); however, the parenchyma cells in *O. crenata* or *S. hermonthica* were located rather closer to or adjacent to host xylem vessels than the parasite xylem bridge. Therefore, the functions of these PP cells in facultative parasites and those described in obligate parasites may differ. In the *S. hermonthica* and rice interaction, we did not find any PP-like cells with thickened cell walls next to the xylem bridge (Figure 2, C). PP cells have been proposed to transfer xylem materials to the hyaline body where xylem-derived materials are transiently stored or processed (Pielach et al., 2014). According to this hypothesis, the function of *P. japonicum* PP cells remains obscure in the absence of an apparent hyaline body. Hyaline body formation relies on host compatibility, as shown in the facultative *R. minor* infecting the incompatible host *Prunella vulgaris* (Pielach et al., 2014). Notably, in this incompatible interaction, *R. minor* is able to develop a xylem bridge, which suggests that hyaline body may have additional function associated with host compatibility compared with the xylem bridge. Although growth of *P. japonicum* benefits from *Arabidopsis* infection (Spallek et al., 2017), it is possible that *Arabidopsis* is not sufficiently compatible with *P. japonicum* for hyaline body formation. Alternatively, the lack of a hyaline body may be a natural feature of *P. japonicum* haustoria.

Xylem connection

The structure of xylem bridges, one of the most conserved features among parasitic plant haustoria, was markedly different between *S. hermonthica* and *P. japonicum*, particularly at the junction points with the host xylem. In *S. hermonthica*, the xylem bridge was perpendicular to the host root, relatively straight, and the interfacing xylem cells made an extreme turn at the tip in the direction parallel to the host root axis (Figure 4, E). This structure probably resulted from the intrusive cells that first inserted between the host xylem precursor cells and later synchronously or successively differentiated into xylem cells with the neighboring host cells. In addition, some intrusive cells of *S. hermonthica* can directly penetrate the xylem vessels of maize and sorghum in a small area of their cell tips by forming oscula (Dörr, 1997). The oscula structures were also observed in our experiment with rice (Figure 2, L). Differentiation of oscula-forming intrusive

cells into vessel elements can eventually lead to xylem continuity (Figure 3, A), providing an oscula-mediated water conducting channel between the host and parasite. Similar connecting structures have been reported in the facultative parasite *Castilleja* (Dobbins and Kuijt, 1973).

Compared with *S. hermonthica*, the xylem bridge of *P. japonicum* is arc shaped with the interfacing xylem curving around the host xylem to eventually target the host xylem in the distal region (Figure 6, E). Such morphology of the interfacing xylem represents the invading direction of intrusive cells because the interfacing xylem is derived from some intrusive cells following the completion of penetration (Figure 3, B). Given that the *Arabidopsis* root is thin, rapid polar growth of intrusive cells might fail to capture the position of the host's central vasculature in the proximal region, and, therefore, growth around the host xylem may be due to guidance toward the host's vasculature. This hypothesis is based on a general assumption that an attraction signal for the tip of intrusive cells may be present in host vasculatures. Such a guidance system is known for pollen tube attraction by synergid cells during pollination, where peptide signals are emitted to attract pollen tubes (Okuda et al., 2009). Interestingly, many haustorial genes are derived from flower genes, suggesting that pollen genes might have been co-opted by the haustorium, as both pollen and haustorial growth involve polar cell growth (Yang et al., 2015; Yoshida et al., 2019). Neither the oscula structures nor the cell wall continuity between the interface xylem and the host xylem was detected at the interface of *P. japonicum* and *Arabidopsis* (Figure 3, B and Supplemental Figure S2). Wrapping the interface xylem around the host xylem vessels increases the interacting surface with host cells; therefore, this phenomenon may contribute toward the efficient acquisition of host xylem contents through xylem pits. A similar interaction was reported in phloem connection of the stem parasite *Cuscuta* and its host, in which the searching hyphal tips grasp the host SE with finger-like protrusions (Dawson et al., 1994). Thus, grasping host vascular cells may be a common feature of parasite intrusive cells (e.g. searching hyphae in dodder) that may have been acquired via convergent evolution.

It should be noted that the different xylem interacting structures observed in *S. hermonthica* and *P. japonicum* do not reflect differences between obligate and facultative parasites nor terminal and lateral haustoria. Oscula structures were observed in the facultative parasites *R. minor* and *Castilleja* (Dobbins and Kuijt, 1973; Cameron et al., 2006), whereas the obligate parasite *O. crenata* and the facultative parasite *T. versicolor* do not form oscula, interacting with host xylem via xylem pits (Dörr and Kollmann, 1976; Heide-Jørgensen and Kuijt, 1993). The vascular connection structures do not associate with host monocot and dicot differences, because *Striga* forms oscula structures on monocot hosts, such as rice, maize, and sorghum, whereas *R. minor* forms oscula on its leguminosae host *Vicia cracca* (Dorr, 1997; Cameron et al., 2006). Thus, the interacting structure

could be determined by parasite species or compatibility with hosts. Observations in different host–parasite combinations are required to formulate general conclusions on the structural characteristics of the xylem connection and its relationship with host dependency.

Discontinuity of SEs between a host and a parasite

Both *S. hermonthica* and *P. japonicum* have SE in the basal region of haustoria in the vicinity of the plate xylem (Figures 2, C and 5, L). Our 3-D reconstruction combined with marker expression analysis revealed that these SEs are connected to phloem strands emanating from the parasite's main vasculature but not to those of the host's roots (Figures 4, D and 6, C). These SEs are interspaced with host phloem by procambium-like cells. A similar observation was reported in *Alectra* where haustorial and host phloem elements are interspaced by haustorial parenchymatic cells (Dörr et al., 1979). Based on electron microscope observations and *pSUC2-GFP* translocation assays, which can visualize intercellular simplistic continuity between host and parasite, phloem connections are thought to occur only in holoparasitic plants (Dörr and Kollmann, 1995; Dörr, 1997; Ekawa and Aoki, 2017; Spallek et al., 2017; Krupp et al., 2019). This observation reflects the importance of phloem-mediated nutrient transfer in holoparasites whose sugar acquisition completely depends on the host. Important questions remain as to how hemiparasites translocate organic compounds with only xylem connections. Tracer experiments with carboxyfluorescein diacetate (CFDA) dye revealed that, although CFDA translocation from the host to the holoparasite *Phelipanche ramosa* is through haustorial phloem strands (Peron et al., 2016), transport to *P. japonicum* is through the inner region of haustoria where intrusive cells and procambium-like cells are located (Spallek et al., 2017). Without characteristic SE in the inner haustorium of hemiparasites, other cell types may function in nutrient delivery either in a symplastic or apoplastic manner.

Procambium-like cells

Our FE-SEM analyses revealed several features in *P. japonicum* procambium-like cells. Vacuoles of procambium-like cells have frequent membrane invaginations and contain many single- or multi-membrane vesicles (Figure 5, G), which indicates active degradation of cytosolic metabolites and organelles. These vesicles are likely associated with vacuole autophagy, a process that can be induced by nutrient starvation or biotic stress, such as pathogen attack (Yu, 1999; Cao et al., 2018; Yoshimoto and Ohsumi, 2018). Whether there is direct functional relevance of the autophagy process in plant parasitism remains to be investigated. In addition, we found two types of procambium-like cells with distinct subcellular features (Figure 5, F). Whereas those in the center and base of the haustorium are highly vacuolated (Figure 5, G), those proximal to the host contain many atypical membrane structures in the cytosol (Figure 5, H). Subtle differences also exist in terms of marker gene expression in the procambium; whereas *PjHB15a*, *PjHB8*, and

PjWOX4 are expressed widely in all procambium-like cells, the expression of *PjHB15b* is limited to the center and basal regions (Wakatake et al., 2018). The identification of additional cell type-specific marker genes is necessary to verify the identities of haustorial cell types in the future.

In summary, we visualized the 3-D structure of haustorium internal cell organization in two Orobanchaceae root parasites, providing the basis for understanding cellular function of haustorial tissues. Expansion of this study for other parasite species, e.g. holoparasites, root parasites from the other family, or stem parasites, and to the other host species, e.g. compatible and non-compatible hosts, or monocot and dicot host interaction with the same parasites, will further reveal association of haustorial internal structures and host dependency or parasitic plant taxonomy. The knowledge will provide a clue to answer the fundamental question of how parasitic plant cells manage host invasion and nutrient absorption.

Materials and methods

Plant materials and growth conditions

The parasitic plants used in this study were *P. japonicum* (Thunb.) Kanitz ecotype Okayama and *S. hermonthica* (Del.) Benth., and the host plants were Arabidopsis (*A. thaliana*) ecotype Columbia (Col-0) and japonica rice (*Oryza sativa* L.) cultivar Koshihikari, respectively. Seed sterilization and host infection were performed as described previously (Cui et al., 2018). Briefly, 1-week preconditioned *S. hermonthica* seeds were treated with 10 nM strigol for 1 d and placed onto rice roots that had been grown using a rhizotron system for 1 week after germinating 1 week on moistened filter paper. The *S. hermonthica*-infected rice plants were grown under long-day conditions (16-h light/8-h dark, 90 $\mu\text{mol m}^{-2} \text{s}^{-1}$) at 25°C for 2 weeks. *Phtheirospermum japonicum* and Arabidopsis were germinated on half-strength Murashige and Skoog (MS) solid media at 25°C and 22°C, respectively, under long-day conditions. Seven-day-old *P. japonicum* seedlings were transferred to a nutrient-free agar medium and cultivated for 3 d under long-day conditions for the starvation treatment. The main root of 7-d-old Arabidopsis seedlings was then placed next to the root of *P. japonicum* to induce infection. One day after infection, successfully induced haustoria were marked; only marked haustoria were collected for sectioning at 9 d after infection. Infection was carried out at 25°C under long-day conditions.

Preparation of serial semi-thin sections of haustoria

Two-week-old *S. hermonthica* haustoria and 9-d-old *P. japonicum* haustoria were collected by excising the roots of the host and parasite 2–3 mm above and below the infection sites. The haustorial samples were fixed with 4% (w/v) formaldehyde, 2% (v/v) glutaraldehyde, and 0.05 M cacodylate buffer, dehydrated in a methanol dilution series, and embedded in EPON 812 resin (TAAB). The resin blocks were sliced with an ultramicrotome (Leica Microsystems EM-UC7) using a diamond knife (DIATOME Histo), and 1- μm -thick serial

sections were prepared. Each slide was stained with 0.05% (w/v) toluidine blue and photographs were taken using an upright light microscope (Olympus BX51M and DP26 digital camera).

FE-SEM observations

Toluidine blue-stained serial sections, prepared as describe above, were stained with a 0.4% (w/v) uranyl acetate solution for 12 min followed by a lead citrate solution for 3 min, dried and coated with osmium for 1 s using an osmium coater (HPC-1SW). Observations and imaging were accomplished using a FE-SEM (Hitachi High-Tech SU 8220) equipped with a highly sensitive backscatter-electron detector (YAG-BSE 5 kV).

3-D reconstruction of surface structures

3-D alignment adjustment

To construct 3-D volumetric images, serial images of toluidine blue-stained sections were adjusted for translation and rotation by rigid image registration using a Python library in SimpleElastix (Marstal et al., 2016). In addition to rigid registration, intensity-based non-rigid image registration was applied to iron out wrinkles in the sectioned images. For non-rigid image registration, wrinkled images were registered to their respective nearest wrinkle-free image. After automated alignment adjustment, section alignment was manually checked and misaligned sections were re-registered by changing the registration parameters. The tools are available at <https://github.com/yk-szk/ssrvtools>.

Semi-automated cell labeling

For color-coding of cell types, a semi-automated labeling method was developed. Each section image was split into RGB channels, and an outline was extracted using the R channel or G channel images using line enhancement and removal of background noise. After line extraction, each line-enclosed area was defined as a single cell. Every fifth slice was subjected to manual painting, in which different cell types within the haustorium were marked manually with different colors using Photoshop CS6 (Adobe) and a tablet pen. A Python script (<https://github.com/yk-szk/ssrvtools>) was developed that automatically paints the intercepted unpainted slices based on information from manually painted images and single cell outlines. The manually painted images and single cell outlines of unpainted images were over-laid, and the color occupying the largest area in the cell was selected to paint the cell. This procedure was repeated up to four times based on one manually painted image. After automatic painting, manual corrections were applied whenever necessary.

Polygon mesh extraction and visualization

Color-painted images were stacked to construct a color-coded 3-D volume image. The surface structure of each cell type was extracted as a polygon mesh using Marching Cubes (Lorensen and Cline, 1987). Extracted polygon meshes

were visualized using the open-source visualization application Paraview (Kitware).

Plasmid construction and transformation

The Arabidopsis *PEAR1* (*AtPEAR1*) promoter sequence was amplified by the primers (5'-TCGACTCTAGAGGATCCCCGGGTGTTGCCTAACTCTTGATTATTGATT-3' and 5'-CCC TTGCTCACCATCCCTGGTTATTCTCTTTTGATTTATTCTCAAAT-3') and cloned into the pAN19 vector by the SLiCE technique (Okegawa and Motohashi, 2015) using the coding sequence of the *tdTomato-NLS* reporter. The *pAtPEAR1::tdTomato-NLS* sequence was inserted into the modified pBIN19 binary vector containing the Basta herbicide resistance gene (Miyashima et al., 2011). The binary vector was transformed into *P. japonicum* seedlings as previously described (Ishida et al., 2016). The binary vector was transformed into *Agrobacterium rhizogenes* strain AR1193. Five-day-old *P. japonicum* seedlings were suspended in the *A. rhizogenes* solution, sonicated, and vacuum infiltrated. The infiltrated seedlings were cultured on Gamborg's B5 medium with 0.5% (w/v) agar, 1% (w/v) sucrose, and 450 μM acetosyringone (Sigma) at 23°C in the dark for 2 d. The seedlings were transferred to Gamborg's B5 medium with 0.5% (w/v) agar, 1% (w/v) sucrose, and 300 $\mu\text{g}/\text{mL}$ cefotaxime (Tokyo Chemical Industry), and then cultured at 25°C under long-day conditions (18 h/6 h for light/dark, 90 $\mu\text{mol m}^{-2} \text{s}^{-1}$) for 18 d, to initiate hairy roots. Initiated hairy roots expressing the fluorescence signal were cultured on the same medium for 2 weeks, and then transferred onto 0.8% (w/v) agar plates for the starvation treatment. After a 1-d starvation treatment, the hairy roots were used to infect Arabidopsis roots. A 2-week-old haustorium expressing a fluorescence signal was observed by Nikon A1 confocal microscopy.

Confocal microscope observation

For xylem staining, haustorial and host root segments were excised from the roots, stained by SR2200 (Renaissance) and Fuchsin, and cleared by ClearSee solution by following previously described protocols with a slight modification (Ursache et al., 2018; Miyashima et al., 2019). The haustorial samples were submerged in 0.1% (v/v) SCRI Renaissance 2200 solution in 1 \times PBS buffer, vacuum infiltrated for 15 min, and incubated at 4°C for 3 d. The sample was then washed once with 1 \times PBS buffer, immersed in 500 μL of ClearSee solution (10% [w/v] xylitol, 15% [w/v] deoxycholate, 25% [w/v] urea) supplemented with 140 μL of 0.2% (v/v) Fuchsin, and placed under vacuum until no bubbles leaked out from the sample. After repeating this step twice, the sample was left at room temperature for 4 h. The solution was then replaced by new ClearSee solution, subjected to a short vacuum treatment, and incubated overnight at room temperature. For imaging, a Zeiss LSM710 confocal microscope was used with excitation and emission wavelengths suitable for blue and red colors.

Accession numbers

Sequence data for AtPEAR1 (AT2G37590) promoter is found in the GeneBank under accession number LR782543.1 (position 16088743-16090273).

Supplemental data

Supplemental Figure S1. Adjustment of coloring borders during automatic interpolation.

Supplemental Figure S2. Xylem–xylem interaction between *P. japonicum* and Arabidopsis.

Supplemental Movie S1. An opaque 3-D structure of *S. hermonthica* haustorium-infected rice.

Supplemental Movie S2. A semi-transparent 3-D structure of *S. hermonthica* haustorium-infected rice.

Supplemental Movie S3. A 3-D internal structure of a *S. hermonthica* haustorium-infected rice.

Supplemental Movie S4. An opaque 3-D structure of *P. japonicum* haustorium-infected Arabidopsis.

Supplemental Movie S5. A semi-transparent 3-D structure of *P. japonicum* haustorium-infected Arabidopsis.

Supplemental Movie S6. A 3-D internal structure of *P. japonicum* haustorium-infected Arabidopsis.

Acknowledgments

The authors thank Dr. A. G. T. Babiker (Environment and Natural Resources and Desertification Research Institute, Sudan) for providing *S. hermonthica* seeds and Dr. Kenji Mori for providing strigol. They also thank Ms. Kana Tsurii (RIKEN) and Dr. Kei Hashimoto (RIKEN) for technical assistance in sample preparation and FE-SEM observation, and Dr. Shunsuke Miyashima (NAIST) for valuable suggestions for microscopy.

Funding

This work was partly supported by the KAKENHI grant numbers 17K15142 and 19K16169 to S.C., 18H02464 and 18H04838 to S.Y., 17H06475 to K.T., 15H05959 and 17H06172 to K.S., JST PRESTO grant number JPMJPR194D to S.Y., and JST CREST grant number JPMJCR1863 to Y.Sa. This study was also partly supported by the International Atomic Energy Agency Research Contract Number 20645.

Conflict of interest statement. The authors declare that they have no conflict of interest.

References

- Ba AT** (1988) Structure et ultrastructure de l'haustorium du *Striga hermonthica*, une scrophulariacée parasite du mil (*Pennisetum typhoides*). *Can J Bot* **66**: 2111–2117
- Behnke HD** (1991) Distribution and evolution of forms and types of sieve-element plastids in the dicotyledons. *Aliso* **3**: 167–182
- Bennett JR, Mathews S** (2006) Phylogeny of the parasitic plant family Orobanchaceae inferred from phytochrome A. *Am J Bot* **93**: 1039–1051
- Bowman JE** (1833) On the parasitical connection of *Lathraea squamaria* and the peculiar structure of the subterranean leaves. *Trans Linn Soc Lond* **16**: 399–420
- Cameron DD, Coats AM, Seel WE** (2006) Differential resistance among host and non-host species underlies the variable success of the hemi-parasitic plant *Rhinanthus minor*. *Ann Bot* **98**: 1289–1299
- Cao J, Zhang M, Xiao J, Li X, Yuan M, Wang S** (2018) Dominant and recessive major R genes lead to different types of host cell death during resistance to *Xanthomonas oryzae* in rice. *Front Plant Sci* **9**: 1711
- Cui S, Kubota T, Nishiyama T, Ishida JK, Shigenobu S, Shibata TF, Toyoda A, Hasebe M, Shirasu K, Yoshida S** (2020) Ethylene signaling mediates host invasion by parasitic plants. *Sci Adv* **6**: eabc2385
- Cui S, Wada S, Tobimatsu Y, Takeda Y, Saucet SB, Takano T, Umezawa T, Shirasu K, Yoshida S** (2018) Host lignin composition affects haustorium induction in the parasitic plants *Phtheirospermum japonicum* and *Striga hermonthica*. *New Phytol* **218**: 710–723
- Cui S, Wakatake T, Hashimoto K, Saucet SB, Toyooka K, Yoshida S, Shirasu K** (2016) Haustorial hairs are specialized root hairs that support parasitism in the facultative parasitic plant *Phtheirospermum japonicum*. *Plant Physiol* **170**: 1492–1503
- Dawson LJ, Musselman LJ, Wolswinkel P, Dörr I** (1994) Biology and control of *Cuscuta*. *Rev Weed Sci* **6**: 265–317
- Dobbins DR, Kuijt J** (1973) Studies on the haustorium of *Castilleja* (Scrophulariaceae). I. The upper haustorium. *Can J Bot* **51**: 917–922
- Dobbins DR, Kuijt J** (1973) Studies on the haustorium of *Castilleja* (Scrophulariaceae). II. The endophyte. *Can J Bot* **51**: 923–931
- Dörr I** (1997) How *Striga* parasitizes its host: a TEM and SEM study. *Ann Bot* **79**: 463–472
- Dörr I, Kollmann R** (1976) Strukturelle Grundlagen des Parasitismus bei *Orobanche* III. Die Differenzierung des Xylemanschlusses bei *O. crenata*. *Protoplasma* **89**: 235–279
- Dörr I, Kollmann R** (1995) Symplasmic sieve element continuity between *Orobanche* and its host. *Bot Acta* **108**: 47–55
- Dörr I, Visser JH, Kollmann R** (1979) On the parasitism of *Alectra vogelii* Benth. (Scrophulariaceae) III. The occurrence of phloem between host and parasite. *Z Pflanzenphysiol* **84**: 213–222
- Ekawa M, Aoki K** (2017) Phloem-conducting cells in haustoria of the root-parasitic plant *Phelipanche aegyptiaca* retain nuclei and are not mature sieve elements. *Plants (Basel)* **6**: 60
- Fineran BA** (1974) A study of 'phloetracheids' in haustoria of santalaceous root parasites using scanning electron microscopy. *Ann Bot* **38**: 937–946
- Goyet V, Wada S, Cui S, Wakatake T, Shirasu K, Montiel G, Simier P, Yoshida S** (2019) Haustorium inducing factors for parasitic Orobanchaceae. *Front Plant Sci* **10**: 1056
- Gurney AL, Slate J, Press MC, Scholes JD** (2006) A novel form of resistance in rice to the angiosperm parasite *Striga hermonthica*. *New Phytol* **169**: 199–208
- Heide-Jørgensen HS** (1991) Anatomy and ultrastructure of the haustorium of *Cassytha pubescens* R Br I the adhesive disk. *Bot Gaz* **152**: 321–334
- Heide-Jørgensen HS** (2013) Introduction: the parasitic syndrome in higher plants. In: D. Joel, J. Gressel, and L. Musselman (eds), *Parasitic Orobanchaceae*, Springer, Berlin, Heidelberg
- Heide-Jørgensen HS, Kuijt J** (1993) Epidermal derivatives as xylem elements and transfer cells—a study of the host–parasite interface in 2 species of *Triphysaria* (Scrophulariaceae). *Protoplasma* **174**: 173–183
- Heide-Jørgensen HS, Kuijt J** (1995) The haustorium of the root parasite *Triphysaria* (Scrophulariaceae), with special reference to xylem bridge ultrastructure. *Am J Bot* **82**: 782–797
- Hjertson ML** (1995) Taxonomy, phylogeny and biogeography of *Lindenbergia* (Scrophulariaceae). *Bot J Linn Soc* **119**: 265–321
- Ishida JK, Wakatake T, Yoshida S, Takebayashi Y, Kasahara H, Wafula E, dePamphilis CW, Namba S, Shirasu K** (2016) Local auxin biosynthesis mediated by a YUCCA flavin monooxygenase

- regulates haustorium development in the parasitic plant *Phtheirospermum japonicum*. *Plant Cell* **28**: 1795–1814
- Joel DM, Bar H, Mayer AM, Plakhine D, Ziadne H, Westwood JH, Welbaum GE** (2012) Seed ultrastructure and water absorption pathway of the root-parasitic plant *Phelipanche aegyptiaca* (Orobanchaceae). *Ann Bot* **109**: 181–195
- Kim G, LeBlane ML, Wafula EK, dePamphilis CW, Westwood JH** (2014) Genomic-scale exchange of mRNA between a parasitic plant and its hosts. *Science* **345**: 808
- Kokla A, Melnyk CW** (2018) Developing a thief: Haustoria formation in parasitic plants. *Dev Biol* **442**: 53–59
- Krupp A, Heller A, Spring O** (2019) Development of phloem connection between the parasitic plant *Orobanche cumana* and its host sunflower. *Protoplasma* **256**: 1385–1397
- Kuijt J** (1977) Haustoria of phanerogamic parasites. *Annu Rev Phytopathol* **15**: 91–118
- Liu N, Shen G, Xu Y, Liu H, Zhang J, Li S, Li J, Zhang C, Qi J, Wang L et al.** (2019) Extensive inter-plant protein transfer between *Cuscuta* parasites and their host plants. *Mol Plant* **13**: 573–585
- Lorensen WE, Cline HE** (1987) Marching cubes: a high resolution 3D surface construction algorithm. *ACM SIGGRAPH Comp Graph* **21**: 163–169
- Marstal K, Berendsen F, Staring M, Klein S** (2016) SimpleElastix: a user-friendly, multi-lingual library for medical image registration. *Proceedings of 29th IEEE Conference on Computer Vision and Pattern Recognition Workshops, (Cvprw 2016)*, 574–582
- Miyashima S, Koi S, Hashimoto T, Nakajima K** (2011) Non-cell-autonomous microRNA165 acts in a dose-dependent manner to regulate multiple differentiation status in the *Arabidopsis* root. *Development* **138**: 2303–2313
- Miyashima S, Roszak P, Sevilem I, Toyokura K, Blob B, Heo JO, Mellor N, Help-Rinta-Rahko H, Otero S, Smet W, et al.** (2019) Mobile PEAR transcription factors integrate positional cues to prime cambial growth. *Nature* **565**: 490–494
- Musselman LJ, Dickson WC** (1975) The structure and development of the haustorium in parasitic Scrophulariaceae. *Bot J Linn Soc* **70**: 183–212
- Mutuku JM, Shirasu K** (2019) *Striga*. *Curr Biol* **29**: 1064–1065
- Ogawa S, Wakatake T, Spallek T, Ishida JK, Sano R, Kurata T, Demura T, Yoshida S, Ichihashi Y, Schaller A, Shirasu K** (2021) Subtilase activity in intrusive cells mediates haustorium maturation in parasitic plants. *Plant Physiol* **185**: 1381–1394
- Okegawa Y, Motohashi K** (2015) A simple and ultra-low cost homemade seamless ligation cloning extract (SLiCE) as an alternative to a commercially available seamless DNA cloning kit. *Biochem Biophys Rep* **4**: 148–151
- Okuda S, Tsutsui H, Shiina K, Sprunck S, Takeuchi H, Yui R, Kasahara RD, Hamamura Y, Mizukami A, Susaki D, et al.** (2009) Defensin-like polypeptide LUREs are pollen tube attractants secreted from synergid cells. *Nature* **458**: 357–361
- Olivier A, Benhamou N, Leroux GD** (1991) Cell surface interactions between sorghum roots and the parasitic weed *Striga hermonthica*: cytochemical aspects of cellulose distribution in resistant and susceptible host tissues. *Can J Bot* **69**: 1679–1690
- Peron T, Candat A, Montiel G, Veronesi C, Macherel D, Delavault P, Simier P** (2016) New insights into phloem unloading and expression of sucrose transporters in vegetative sinks of the parasitic plant *Phelipanche ramosa* L. (Pomel). *Front Plant Sci* **7**: 2048
- Pielach A, Leroux O, Domozych DS, Knox JP, Popper ZA** (2014) Arabinogalactan protein-rich cell walls, paramural deposits and ergastic globules define the hyaline bodies of rhinanthoid Orobanchaceae haustoria. *Ann Bot* **114**: 1359–1373
- Runo S, Kuria EK** (2018) Habits of a highly successful cereal killer, *Striga*. *PLoS Pathog* **14**: e1006731
- Shahid S, Kim G, Johnson NR, Wafula E, Wang F, Coruh C, Bernal-Galeano V, Phifer T, dePamphilis CW, Westwood JH, et al.** (2018) MicroRNAs from the parasitic plant *Cuscuta campestris* target host messenger RNAs. *Nature* **553**: 82–85
- Smith JD, Mescher MC, De Moraes CM** (2013) Implications of bio-active solute transfer from hosts to parasitic plants. *Curr Opin Plant Biol* **16**: 464–472
- Spallek T, Melnyk CW, Wakatake T, Zhang J, Sakamoto Y, Kiba T, Yoshida S, Matsunaga S, Sakakibara H, Shirasu K** (2017) Interspecies hormonal control of host root morphology by parasitic plants. *Proc Natl Acad Sci U S A* **114**: 5283–5288
- Spallek T, Mutuku M, Shirasu K** (2013) The genus *Striga*: a witch profile. *Mol Plant Pathol* **14**: 861–869
- Ursache R, Andersen TG, Marhavy P, Geldner N** (2018) A protocol for combining fluorescent proteins with histological stains for diverse cell wall components. *Plant J* **93**: 399–412
- Visser JH, Dörr I, Kollmann R** (1984) The hyaline body of the root parasite *Alectra orobanchoides* Benth (Scrophulariaceae)—its anatomy, ultrastructure and histochemistry. *Protoplasma* **121**: 146–156
- Wakatake T, Yoshida S, Shirasu K** (2018) Induced cell fate transitions at multiple cell layers configure haustorium development in parasitic plants. *Development* **145**: dev164848
- Westwood JH, Yoder JI, Timko MP, dePamphilis CW** (2010) The evolution of parasitism in plants. *Trends Plant Sci* **15**: 227–235
- Yang ZZ, Wafula EK, Honaas LA, Zhang HT, Das M, Fernandez-Aparicio M, Huang K, Bandaranayake PCG, Wu B, Der JP, et al.** (2015) Comparative transcriptome analyses reveal core parasitism genes and suggest gene duplication and repurposing as sources of structural novelty. *Mol Biol Evol* **32**: 767–790
- Yoshida S, Cui S, Ichihashi Y, Shirasu K** (2016) The haustorium, a specialized invasive organ in parasitic plants. *Annu Rev Plant Biol* **67**: 643–667
- Yoshida S, Kim S, Wafula EK, Tanskanen J, Kim YM, Honaas L, Yang Z, Spallek T, Conn CE, Ichihashi Y, et al.** (2019) Genome sequence of *Striga asiatica* provides insight into the evolution of plant parasitism. *Curr Biol* **29**: 3041–3052.e3044
- Yoshida S, Shirasu K** (2009) Multiple layers of incompatibility to the parasitic witchweed, *Striga hermonthica*. *New Phytol* **183**: 180–189
- Yoshimoto K, Ohsumi Y** (2018) Unveiling the molecular mechanisms of plant autophagy from autophagosomes to vacuoles in plants. *Plant Cell Physiol* **59**: 1337–1344
- Yu SM** (1999) Cellular and genetic responses of plants to sugar starvation. *Plant Physiol* **121**: 687–693